IEEE Access
Multidisciplinary ⋮ Rapid Review ⋮ Open Access Journal

Received February 4, 2022, accepted February 14, 2022, date of publication February 17, 2022, date of current version February 28, 2022.

Digital Object Identifier 10.1109/ACCESS.2022.3152704

Clustered Double-Scattering Channel Modeling for XL-MIMO With Uniform Arrays

DAVID WILLIAM MARQUES GUERRA AND TAUFIK ABRÃO, (Senior Member, IEEE)
Department of Electrical Engineering. State University of Londrina, Parana 86057-970, Brazil

Corresponding author: Taufik Abrão (taufik@uel.br)

This work was supported in part by the Coordenação de Aperfeiçoamento de Pessoal de Nível Superior (CAPES) under Grant Financial Code 001, and in part by the National Council for Scientific and Technological Development (CNPq) of Brazil under Grant 310681/2019-7.

ABSTRACT Extra-large multiple-input multiple-output (XL-MIMO) systems reveal themselves as a potential candidate for the sixth generation (6G) of wireless communication systems due to their features. As XL-MIMO has a large antenna array, and, typically, the urban environment is plenty of obstacles and reflectors, the spatial non-stationarities are introduced in the signal received at the base station (BS), which means that only a portion of the antenna array is visible to users; hence, accurately modeling XL-MIMO channels is paramount. Previous works on XL-MIMO channel modeling have adopted the non-stationarities only in a spatial sense, and do not consider spatial-time evolution scenarios. Moreover, simplified models with only one set of clusters between the BS and the user equipment (UE) are usually adopted; hence, there is a lack of understanding regarding such channels modeling in the literature. This work proposes and extensively analyzes a double-scattering XL-MIMO channel model, by admitting two types of scattering clusters, one placed at the BS side, and another one located near the UEs. In addition, two distinct antenna array configurations are included in the analysis, the uniform linear and planar arrays (ULA and UPA). We propose a new double-scattering channel model under UPA arrangements, suitable for modeling spatial non-stationarities scenarios in XL-MIMO dynamic environment subject to BS-cluster and UE-cluster correlation, and birth-death channel clusters and scatterers. Numerical results for signal-to-interference-plus-noise ratio (SINR), condition number (CN), and spectral efficiency (SE) performance metrics considering different XL-MIMO channels and system configurations are analyzed via Monte-Carlo simulations, under linear combiners MRC, ZF, and MMSE. Also, we characterize the impact of the number of visible clusters per user, the birth-death rate growth effect on the channel clusters and scatterers, and the favorable propagation effect according to the size of visibility region (VR) overlap. It can be observed that the birth and death processes have a significant impact on the system performance. Under the proposed clustered double-scattering channel modeling, the analyzed XL-MIMO linear receivers presented an SINR degradation around 3 to 4 dB for the MMSE when the number of UEs substantially increased, while the ZF and MRC receivers present a decrease of 1 to 2 dB, approximately, in SINR for the considered dynamic configuration compared with static scenarios.

INDEX TERMS Uniform linear array (ULA), uniform planar array (UPA), extra large MIMO (XL-MIMO), channel modeling, spatial non-stationary, visibility region, birth and death Poisson process (BDPP).

I. INTRODUCTION

Extra-large multiple-input multiple-output (XL-MIMO) is a promising research direction of multi-antenna technology for the sixth-generation (6G) of wireless communication networks [1]–[3]. The main idea of XL-MIMO is to employ a significant number of antennas (10^3 or more) at the base station (BS), which can be widely spread, *e.g.*, on the walls of dense buildings in the city, roof of airports, public open spaces, walls of stadiums, etc. This system is thus able to serve multiple user equipments (UEs) simultaneously, achieving a substantial increase of spectral efficiency (SE) thanks to the high spatial multiplexing gain. It is well-known in the literature that when the number of antennas increases the array becomes physically large and takes advantage of some benefits, including channel hardening, asymptotic

The associate editor coordinating the review of this manuscript and approving it for publication was Faissal El Bouanani.

favorable propagation, and area throughput [4]. These features promised by massive multiple-input multiple-output (mMIMO) can be fully harnessed from a theoretical point of view and extended to the XL-MIMO context with some adaptations. Basically, when the number of antennas becomes very large, spatial non-stationarities emerge. In other words, when the dimension of the antenna array becomes very large, the far-field propagation assumption is no longer valid, since the distance between the BS and the scatterers/clusters or users is smaller than the Rayleigh distance [5]. This fact implies that users can see only a physical portion of the BS antenna array due to the limited energy dispersion of the propagation paths and the array dimensions. The portion of the antenna array in the BS seen by users is called by visibility region (VR) [6]. As there is still a lack of understanding of the XL-MIMO propagation environment, further researches on channel modeling and system-level performance evaluation are highly required. Indeed, such knowledge is paramount in the design of efficient signal processing techniques for communications aided by extra-large arrays [7], [8]. In the XL-MIMO context, we have very specific physical characteristics that should be covered by the wireless channel model adopted, *e.g.*, non-stationarities and near-field propagation, which directly impact the wireless channel modeling and other important channel metrics [9], [10]. An important factor for modeling the channel propagation in XL-MIMO is the effects caused by obstacles, such as buildings and trees, which can be represented by scattering points. In general, there are two classic types of statistical channel models, the correlation-based stochastic models (CBSM), in which a correlation factor only models the correlation degree, and the geometry-based stochastic models (GBSM) that take into account the effects of certain propagation geometry parameters, such as the distribution of the scatterers and their locations around the transmitters and receivers; such distribution results in a correlation degree between the antennas. Therefore, although CBSM models are less complex than the GBSM one, some environmental features are not entirely captured with the CBSM models. Consequently, the GBSM is more accurate for describing specific scenarios, such as mMIMO and XL-MIMO [11].

Recent researches on wireless channel modeling have included non-stationary properties [11]–[13]. In [11], stochastic channel models for mMIMO and XL-MIMO systems are described, evaluated, and compared. More specifically, in the case of the XL-MIMO channel, the one-ring model is analyzed using metrics such as capacity and SINR. Additionally, the correlation effect due to the location of the clusters is evaluated in the performance of linear precoding schemes. In [12], a three-dimensional (3D) wireless channel model for vehicle-to-vehicle (V2V) communication environments is presented adopting the spherical wavefront assumption, while the non-stationarity property is only considered in a temporal sense. In [13], a double-scattering channel model is presented for a linear array in the XL-MIMO context, also taking into account the near-field propagation with the spherical wavefront, including the spatial non-stationarity properties for the system with the VR concept. However, the work is restricted to the uniform linear array (ULA) and the space-time evolution of scatterers/clusters is neglected, considering only a static perspective.

In addition, some research works have adopted *birth and death processes* to model the channel non-stationarities [14]–[18]. Both [14], [15] propose a one-ring mMIMO channel model, where there is only one set of clusters near the BS. A birth and death process of channel clusters is incorporated to reproduce non-stationary properties of clusters on both the array and time axes. While in [14] the VR of each cluster is obtained from the ray visibility gain to the receive antennas, in [15] the mean power updates of rays are embedded in the small-scale fading channel model with the assumption of the inverse square law, not considering the VR effect. Authors in [16] propose a transformation method to model space-time-variant (STV) two-dimensional non-stationary wideband mMIMO channels considering the disappearance of multipath components (MPCs) and the drift and spread of the time of arrival over the array. In this case, only a set of scatterers are implemented with a specific distribution governed by a birth and death process. López *et al.* [17] updated [16] to a 3D wideband mMIMO channel model, where statistical properties are derived. In this work, the scatterers are clustered and now a Poisson process determines the appearance/disappearance of these clusters to capture array-variant characteristics, such as the VR effect. Lastly, in [18] a GBSM non-stationary channel model operating at millimeter wave (mmWave) is proposed for unmanned aerial vehicle (UAV) MIMO communications, where is considered both local and far clusters, in which a continuous-time Markov model is adopted to model the dynamic properties of the clusters, *i.e.*, the appearance/disappearance of clusters over time.

Channel measurements provided in [19] highlight the complexity of modeling XL-MIMO channels. In this work, a very large variation in power that reaches the array (more than 10dB) and different patterns for signals coming from each device were observed. Therefore, the non-stationary properties of XL arrays indicate that a substantial modification on the widely used correlated channel model is needed in order to consider the variation on the average channel gain along with the array. A clustered double-scattering channel model can reflect more appropriately the effects of the non-stationarity phenomenon in XL arrays since it depends on both spatial correlations at the communication endpoints, as well as on the scattering structure along the propagation environment.

Against this background, we emphasize that the works in the literature previously mentioned do not present a specific and accurate channel model accurately describing the XL-MIMO scenario and effects, including non-stationarities, correlation, and near-field effect. Therefore, the descriptions and models on the XL-MIMO channel found in the literature

are incipient yet, requiring further discussion, since it is crucial to achieve a better understanding on the XL-MIMO channel and system. To the best of our knowledge, non-stationary properties of clusters and scatterers in XL-MIMO correlated channel modeling with distributed scattering have not been comprehensively analyzed in the literature.

The *contribution* of this work is threefold.

- We propose a dedicated channel modeling for XL-MIMO systems, where the BS is equipped with XL uniform linear and planar arrays (ULA and UPA). For that, a double-scattering channel model is considered. There are two scattering clusters; one emerges stochastically near the BS side, while the second cluster also stochastically appears near the user side. Such specific channel model has been conceived for XL-MIMO structures, based on current appealing scenarios of application in 5G, including crowded system and channel configurations subject to many obstacles, typically found in urbanized environments.
- We have modeled the birth and death of the correlated BS-cluster and UE-cluster, as well as the scatterers, via Poisson processes, generating a space-time evolutionary process of scatterers/clusters that results in quasi-static and dynamic spatial correlated XL-MIMO channels.
- Extensive numerical results corroborate the validity of the proposed XL-MIMO channel modeling methodology by comprehensively evaluating the effect of birth and death Poisson point processes (PPP) and Poisson clustering process (PCP), the effect of interference, channel correlation, and the spectral efficiency of an XL-MIMO system equipped with UPA or ULA and linear combiners at the receiver. Besides, we analyse the impact of parameters choice of a double-scattering correlated quasi-static or dynamic channels under XL-UPA and XL-ULA arrays via condition number of channel matrix and attainable average SINR, also considering different linear combiners.

The remainder of this paper is organized as follows. Section II describes the adopted multiuser XL-MIMO system model. The XL-MIMO channel modeling considering linear and planar arrays are also discussed in section II. Numerical results corroborating the validity of the proposed channel models are explored in section IV. Section V concludes the paper.

Notation: operator $\otimes$ represents the Kronecker product, and tr$(\cdot)$ is the trace of a matrix. $[\cdot]^T$ holds for the transpose operator. diag$(\cdot)$ is the diagonal operator, while $[\cdot]^H$ denotes Hermitian operator, $\mathbf{I}_M$ is an identity matrix of size $M \times M$. $\|\cdot\|$ means Frobenius norm, while $|\cdot|$ is the modulus operator. $\mathbb{E}\{\cdot\}$ denotes expectation operator; $\mathbb{V}ar\{\cdot\}$ denotes variance operator; $\lceil\cdot\rceil$ denotes the nearest integer greater than or equal of a real value; $j = \sqrt{-1}$ is the complex number; capital calligraphic letters denote finite sets; bold lowercase letter represents a vector, while bold capital letter represents matrix. $[\cdot]_{(m,n)}$ represent the element of the mth row and nth column of a matrix. $x \sim \mathcal{CN}(\overline{x}, \sigma_x^2)$ represents a random variable x with a circularly symmetric complex Gaussian distribution, where $\overline{x}$ and σ_x^2 are the mean and variance of x, respectively. $\mathcal{U}(a, b)$ is a uniform distribution in [a; b] interval. $x \sim \mathcal{LN}(\mu_x, \sigma_x)$ is a random variable x with log-normal distribution, where μ_x and σ_x denote the distribution parameters.

II. XL-MIMO CHANNEL MODELING

In the XL-MIMO system, different channel conditions are obtained due to the close distance between array and user and the use of extremely large arrays. Thus, the far-field propagation of the electromagnetic wave is no longer valid. In this case, the array will experience spherical wavefronts instead of planar wavefronts, which characterizes the near-field propagation. Hence, the concept of spatial non-stationarity is introduced together with VR, double-scattering clusters, and near-field wave propagation aiming to suitably describe the XL-MIMO channel [8].

Assuming narrow-band transmissions, the received base-band signal $\mathbf{y} \in \mathbb{C}^{M\times 1}$ across the whole array is defined as:

$$\mathbf{y} = \mathbf{H}\mathbf{x} + \mathbf{n}, \tag{1}$$

in which $\mathbf{x} \in \mathbb{C}^{K\times 1}$ denotes the vector of complex input symbols with normalized power $\mathbb{E}[\mathbf{x}^2] = 1$; besides, the complex channel matrix can be defined as

$$\mathbf{H} = [\mathbf{h}_1, \ldots, \mathbf{h}_K] \in \mathbb{C}^{M\times K}, \tag{2}$$

where $\mathbf{h}_k$ is the channel between the kth user and the BS, defined in the following section, eq. (3); finally, the AWG noise is a random variable modeled by a complex Gaussian distribution $\mathbf{n} \sim \mathcal{CN}(0, \sigma_n^2\mathbf{I}_M)$.

In the next subsections, two different antenna arrangements of interest in practical application scenarios for multi-user XL-MIMO wireless communications are explored, *i.e.*, ULA and UPA.

A. CLUSTER VR AND CORRELATION IN ULA

Let $\mathbf{h}_k \in \mathbb{C}^{M\times 1}$ denote the kth column of $\mathbf{H}$, corresponding to user k. Additionally, let K denote the number of users simultaneously active, which are single antenna equipped.

In order to model the channel in a generic way, the double scattering model is considered [13]. The double scattering concept defines two types of scattering clusters placed at the BS side called BS-cluster and another located near the user side called U-cluster. In this channel, the spatial correlation at the transmitter and receiver is separable. Additionally, we assume that there are C clusters at the BS side and only one cluster for each user.

We are assuming that the VR of each cluster is greater than or equal to 50 antennas, on average. Therefore, all users in front of the BS uniform array attain the massive MIMO condition; hence, both massive antenna reception properties namely *channel hardening* and *favorable propagation* are satisfied. Under such a channel condition, small-scale fading disappears within each VR, while large-scale effects dominate. However, in the adopted typical XL-MIMO geometric scenarios, the geographic distribution of UEs occurs in front

of and close to the extension of the ULA or UPA panel, with similar distances and much smaller than the length of the uniform array. Therefore, in this case, the large-scale coefficients of each user do not differ significantly.

In this context, we can model the channel between the kth user and the BS as follows:

$$\mathbf{h}_k = [\tilde{\mathbf{H}}_{1,k}, \cdots, \tilde{\mathbf{H}}_{C,k}]\mathbf{D}_k\mathbf{g}_k, \quad \forall\, k \in \{1, \ldots, K\}, \tag{3}$$

where $\tilde{\mathbf{H}}_{i,k} \in \mathbb{C}^{M\times S_i}$ represents the sub-channel between the ith BS-cluster with S_i scatterers for the kth user, $\mathbf{D}_k \in \mathbb{C}^{S'\times S_k}$ is responsible for defining which BS-clusters are visible to the U-cluster of the kth user, and $\mathbf{g}_k \sim \mathcal{CN}(0, 1) \in \mathbb{C}^{S_k\times 1}$ denotes the small-scale fading between the kth user and the S_k scatterers presents in its U-cluster. Furthermore, we assume that S' constitutes the visible scatterers at the BS side w.r.t. the U-cluster, *i.e.*, $S' = \sum_{i=1}^{C} S_i$.

We formulate the sub-channel between the ith BS-cluster and the U-cluster related to the kth user as

$$\tilde{\mathbf{H}}_{i,k} = \Upsilon_i\boldsymbol{\rho}_i^{\frac{1}{2}}\mathbf{R}_i^{\frac{1}{2}}\mathbf{G}_i\tilde{\mathbf{R}}_{i,k}^{\frac{1}{2}}, \tag{4}$$

where $\Upsilon_i \in \{0, 1\}^{M\times r_i}$ indicates which BS antennas are visible to the ith BS-cluster, since r_i is the number of visible antennas, $\boldsymbol{\rho}_i \in \mathbb{C}^{r_i\times r_i}$ represents the visibility power (energy) gain, $\mathbf{R}_i \in \mathbb{C}^{r_i\times r_i}$ the correlation matrix between the BS and the ith BS-cluster, $\mathbf{G}_i \in \mathbb{C}^{r_i\times S_i}$ is the complex scattering amplitudes between the BS and the ith BS-cluster and $\tilde{\mathbf{R}}_{i,k} \in \mathbb{C}^{S_i\times S_i}$ is the correlation matrix between the ith BS-cluster and the U-cluster for the kth user. Next, each channel component presented in equations (3) and (4) will be explained in more detail.

1) CLUSTER VR (Υ_i)

The set of BS antennas that are visible to a given BS-cluster defines the cluster VR concept in this channel propagation model. Therefore, this set contains the indexes of the antennas that are visible to each BS-cluster channel, which is denoted by $\mathcal{R}_i = \{a_1^i, \cdots, a_{r_i}^i\}$, where a_l^i is the index of the lth antenna element inside the ith BS-cluster VR.

$$\Upsilon_i = \begin{bmatrix} \mathbf{0}_{m_i'\times r_i} \\ \mathbf{I}_{r_i} \\ \mathbf{0}_{m_i''\times r_i} \end{bmatrix}, \tag{5}$$

where $\mathbf{0}_{m_i\times r_i}$ are zero matrices with $m_i' = a_1^i - 1$ and $m_i'' = M - a_{r_i}^i$ and $\mathbf{I}_{r_i}$ is the identity matrix of dimensions $r_i \times r_i$. If we have, *e.g.*, a system with $M = 7$ antennas and a BS-cluster ($i = 1$) that has a VR defined by the set $\mathcal{R}_1 = \{3, 4, 5\}$, the matrix $\Upsilon_1 \in \{0, 1\}^{7\times 3}$ can be written as follows:

$$\Upsilon_1 = \begin{bmatrix} 0 & 0 & 0 \\ 0 & 0 & 0 \\ 1 & 0 & 0 \\ 0 & 1 & 0 \\ 0 & 0 & 1 \\ 0 & 0 & 0 \\ 0 & 0 & 0 \end{bmatrix}.$$

2) POWER DISTRIBUTION (ρ_i)

Due to the spherical wavefront propagation inherent to the XL-MIMO system, the power that arrives in each antenna of the subarray that forms the ith cluster VR is not equally distributed, as shown from practical measurements performed on [20]. As a result of this physical effect, the energy peak occurs at the center of the visibility region, and then it is attenuated linearly with a constant rate ψ_i (dBm^{-1}) inside the VR. Hence, the energy distribution matrix for the ith cluster VR can be represented by $\boldsymbol{\rho}_i = \text{diag}(\rho_i[1], \ldots, \rho_i[r_i]) \in \mathbb{C}^{r_i\times r_i}$. Additionally, this visibility gain matrix of the nth antenna included in the VR can be evaluated using a discrete function such as:

$$\rho_i[n] = 10^{-\psi_i|a_{c_i}^i - a_n^i|d_r}, \quad \forall\, n \in \{1, \ldots, r_i\}, \tag{6}$$

where $a_{c_i}^i = \lceil \frac{a_1^i + a_{r_i}^i}{2} \rceil$ denotes the index of the antenna located in the center of the ith cluster VR, a_n^i is the index of the nth antenna included in this VR, while d_r represents the BS antenna spacing in multiples of the signal wavelength.

3) CORRELATION BETWEEN THE BS AND THE ith BS-CLUSTER ($\mathbf{R}_i$)

The correlation between the receiver side (BS antennas) and the ith BS-cluster is defined by the correlation matrix $\mathbf{R}_i \in \mathbb{C}^{r_i\times r_i}$, which its (m, n) element can be evaluated as follows:

$$[\mathbf{R}_i]_{(m,n)} = \frac{1}{S_i}\sum_{\ell=\frac{1-S_i}{2}}^{\frac{S_i-1}{2}} e^{-2\pi j d_r(m-n)sin\left(\alpha_i + \frac{\ell\theta_i}{S_i-1}\right)}, \tag{7}$$

where α_i represents the azimuth angle, while θ_i is the angular spread between the BS and the ith BS-cluster.

4) CORRELATION BETWEEN THE ith BS-CLUSTER AND THE U-CLUSTER FOR THE kth USER ($\tilde{\mathbf{R}}_{i,k}$)

Assuming that we have S_k scatterers at the kth U-cluster, these scatterers can be represented as a virtual antenna array with S_k elements and an average spacing d_s in multiples of the wavelength. Therefore, the (m, n) element of the correlation matrix between the ith BS-cluster and the U-cluster can be obtained as:

$$[\tilde{\mathbf{R}}_{i,k}]_{(m,n)} = \frac{1}{S_i}\sum_{\ell=\frac{1-S_i}{2}}^{\frac{S_i-1}{2}} e^{-2\pi j d_s(m-n)sin\left(-\tilde{\alpha}_{i,k} + \frac{\ell\tilde{\theta}_{i,k}}{S_i-1}\right)}, \tag{8}$$

where $\tilde{\alpha}_{i,k}$ is the azimuth angle and $\tilde{\theta}_{i,k}$ denotes the corresponding angular spread between the ith BS-cluster and the U-cluster of user k.

5) VISIBILITY MATRIX ($\mathbf{D}_k$)

Another type of VR considered in this propagation environment is the U-cluster VR for each k user. This user VR is represented by a set of clusters that are visible for the kth user, denoted by $\mathcal{V}_k$. The practical mean of the user VR is that only part of the C BS-clusters is visible to each k U-cluster.

Moreover, we need to define the scatterer visibility set $\mathcal{C}_k$, which can be seen as being a set that contains all the indexes representing the visible scatterers of the BS-clusters in $\mathcal{V}_k$ related to the kth user. Thus, the mth row of the visibility matrix $\mathbf{D}_k \in \mathbb{C}^{S' \times S_k}$ is obtained as:

$$[\mathbf{D}_k]_{(m,:)} = \begin{cases} \mathbf{1}, & \text{if } m \in \mathcal{C}_k \\ \mathbf{0} & \text{otherwise} \end{cases} . \tag{9}$$

For example, considering 4 BS-clusters with 3 scatterers each, a U-cluster ($k = 1$) with 6 scatterers and the user VR set given by $\mathcal{V}_1 = \{2, 4\}$. Therefore, the set representing the scatterer visibility is written as $\mathcal{C}_1 = \{4, 5, 6, 10, 11, 12\}$ and the visibility matrix is

$$\mathbf{D}_1 = \begin{bmatrix} 0 & 0 & 0 & 0 & 0 & 0 \\ 0 & 0 & 0 & 0 & 0 & 0 \\ 0 & 0 & 0 & 0 & 0 & 0 \\ 1 & 1 & 1 & 1 & 1 & 1 \\ 1 & 1 & 1 & 1 & 1 & 1 \\ 1 & 1 & 1 & 1 & 1 & 1 \\ 0 & 0 & 0 & 0 & 0 & 0 \\ 0 & 0 & 0 & 0 & 0 & 0 \\ 0 & 0 & 0 & 0 & 0 & 0 \\ 1 & 1 & 1 & 1 & 1 & 1 \\ 1 & 1 & 1 & 1 & 1 & 1 \\ 1 & 1 & 1 & 1 & 1 & 1 \end{bmatrix} .$$

Fig. 1 illustrates the scenario considered for the XL-MIMO with the ULA arrangement. Blue points represent the scatterers, while a set of near-scatterers forms a cluster. Furthermore, the shading elements (scatterers and clusters) represent the evolution of the scenario based on the birth and death Poisson process described in more detail in section II-C.

B. CLUSTER VR, POWER DISTRIBUTION AND CORRELATION I UPA

Consider a planar antenna array in the y-z-plane with $M = M_z \times M_y$ antennas, where M_z represents the horizontal rows each with M_y antennas. In this case, the antennas are uniformly spaced with vertical and horizontal spacing d_z and d_y (given in multiples of the wavelength), respectively, as shown in Fig. 2. Moreover, the antennas are indexed row-by-row, so that $\mathbf{u}_m \in R^3$ is the location of the mth antenna ($m = 1, \ldots, M$) on the x, y, and z axis for the planar arrangement, which can be described as:

$$\mathbf{u}_m = \begin{bmatrix} 0 \\ p_y(m) \\ p_z(m) \end{bmatrix}, \tag{10}$$

where $p_y(m) = \mod(m-1, M_h)d_h$ and $p_z(m) = \lfloor (m-1)/M_h \rfloor d_v$ are the horizontal and vertical position of antenna m, respectively.

In this context, we can model the channel between the kth user and the BS similarly to eq. (3) rewriting some terms to adapt the formulation to the new geometry of the scenario considered. So we need to reformulate the matrices presented in eq. (4), which denotes the sub-channel between the ith BS-cluster and the U-cluster.

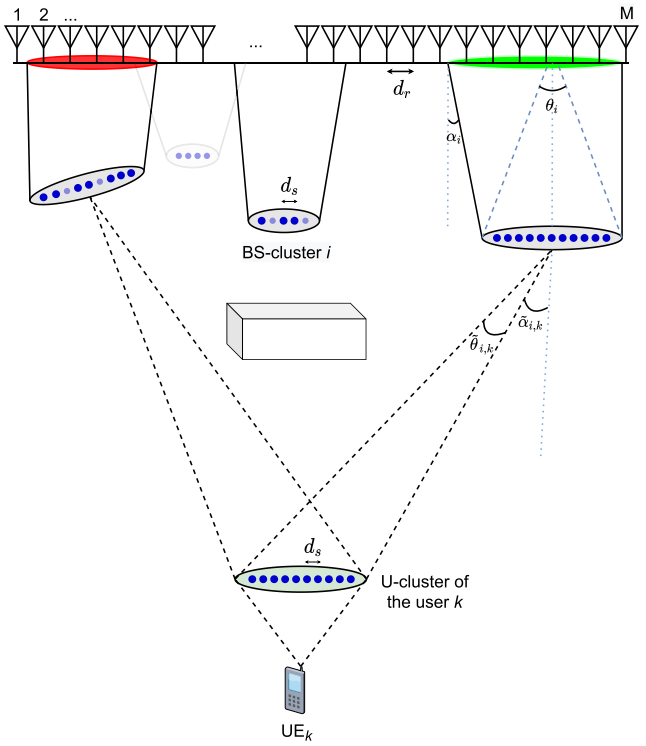

FIGURE 1. XL-MIMO array with spatial non-stationary regions along the ULA with double-scattering channel modeling: ith BS-cluster, with $i = 1, 2, \ldots C$, and kth U-cluster.

1) CLUSTER VR (Υ_i)

Similarly to the ULA case, the matrix $\Upsilon_i \in \{0, 1\}^{M \times r_i}$ denotes the set of BS antennas that are visible to a given BS-cluster, by introducing the VR cluster concept in this channel model. The set containing the indexes of the antennas that are visible to each BS-cluster is denoted by $\mathcal{R}_i = \{a_1^i, \cdots, a_{r_i}^i\}$, where a_n^i is the index of the nth antenna element inside the ith BS-cluster VR. However, as antennas are now indexed row-by-row the cluster VR for the planar array is written as:

$$[\Upsilon_i]_{(a_n^i, n)} = \begin{cases} 1, & \forall \quad n \in \{1, \ldots, r_i\} \\ 0 & \text{otherwise} \end{cases} . \tag{11}$$

2) POWER DISTRIBUTION (ρ_i)

The energy distribution for the UPA scenario differs from the ULA case due to the geometry of the problem, since now we have to consider both y and z coordinates. Hence, the energy distribution matrix for the ith cluster VR can also be represented by $\boldsymbol{\rho}_i = \text{diag}(\rho_i[1], \ldots, \rho_i[r_i]) \in \mathbb{C}^{r_i \times r_i}$, and the power received by the nth antenna inside the VR is obtained as follows:

$$\rho_i[n] = 10^{-\psi_i \sqrt{\left[p_y(a_{c_i}^i) - p_y(a_n^i)\right]^2 + \left[p_z(a_{c_i}^i) - p_z(a_n^i)\right]^2}}, \tag{12}$$

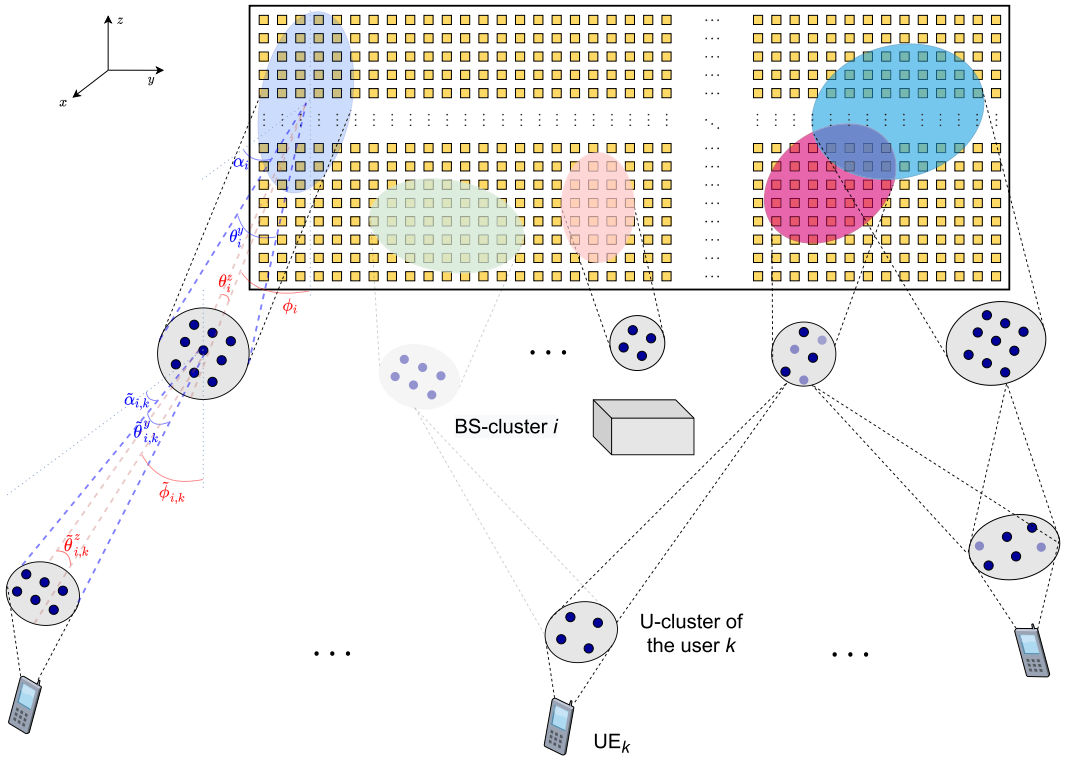

FIGURE 2. XL-MIMO configuration highlighting the spatial non-stationary regions along with the UPA, and the double-scattering entities, where for each UE-BS link, one cluster appears near to each UE and the other rises near to the BS. Shading elements (scatterers and clusters) represent the death in the Poisson process.

$\forall n \in \{1, \ldots, r_i\}$, where ψ_i is the attenuation factor (dB/m) for the ith BS-cluster, p_y and p_z are the coordinates in the y and z axes, respectively, as represented in eq. (10).

3) CORRELATION BETWEEN UPA AND ith BS-CLUSTER ($\mathbf{R}_i$)

This correlation matrix can be obtained by the Kronecker product between two ULA correlation matrices [21]. From the UPA antenna configuration, having M_z antenna elements along the Z coordinate and M_y along the Y coordinate results in an with $M = M_z \times M_y$ antennas. Hence, considering that the correlation between the elements along the Z coordinate given by matrix $\mathbf{R}_i^z$ does not depend on Y and, similarly, the correlation along the Y coordinate ($\mathbf{R}_i^y$) does not depend on Z, the Kronecker model approximation for the UPA correlation matrix can be written as:

$$\mathbf{R}_i = \mathbf{R}_i^y \otimes \mathbf{R}_i^z, \tag{13}$$

where $\otimes$ is the Kronecker product.

Notice that $\mathbf{R}_i^y$ and $\mathbf{R}_i^z$ refer to a subset of the BS antenna array (concerning the Y and Z coordinates, respectively), forming ULA visible region arrangements in both directions. Hence, one can consider the number of scatterers in each direction, independently, for the corresponding ULA arrangements, *i.e.*, S_i^y and S_i^z scatterers along Y and Z coordinates, respectively, for the ith BS-cluster. Therefore, these matrices can be calculated in a similar way as in eq. (7), resulting in:

$$[\mathbf{R}_i^y]_{(m,n)} = \frac{1}{S_i^y} \sum_{\ell=\frac{1-S_i^y}{2}}^{\frac{S_i^y-1}{2}} e^{-2\pi j d_y (m-n) \sin\left(\alpha_i + \frac{\ell\theta_i^y}{S_i^y-1}\right)}, \tag{14}$$

where α_i represents the azimuth angle, while θ_i^y is the angular spread along Y coordinate between the BS and the ith BS-cluster.

$$[\mathbf{R}_i^z]_{(m,n)} = \frac{1}{S_i^z} \sum_{\ell=\frac{1-S_i^z}{2}}^{\frac{S_i^z-1}{2}} e^{-2\pi j d_z (m-n) \sin\left(\phi_i + \frac{\ell\theta_i^z}{S_i^z-1}\right)}, \tag{15}$$

where ϕ_i is the elevation angle and θ_i^z denotes the angular spread in the Z coordinate between the BS and the ith BS-cluster.

4) CORRELATION BETWEEN THE ith BS-CLUSTER AND THE U-CLUSTER FOR THE kth USER ($\tilde{\mathbf{R}}_{i,k}$)

In order to model this correlation matrix, the same principle as the ULA scenario was adopted, for simplicity. Considering that each U-cluster has S_k scatterers, these scatterers can be seen as a virtual antenna array, but now with a UPA arrangement of S_k antenna elements. Therefore, the (m,n)-th element of the correlation matrix between the ith BS-cluster and the kth U-cluster can be obtained as:

$$\tilde{\mathbf{R}}_{i,k} = \tilde{\mathbf{R}}_{i,k}^y \otimes \tilde{\mathbf{R}}_{i,k}^z, \tag{16}$$

where $\tilde{\mathbf{R}}^{y}_{i,k}$ and $\tilde{\mathbf{R}}^{z}_{i,k}$ are the correlation matrices corresponding to the virtual ULA arrangements considered separately, *i.e.*, w.r.t. the Y and Z coordinates, respectively. Hence, these correlation matrices can be evaluated as:

$$[\tilde{\mathbf{R}}^{y}_{i,k}]_{(m,n)} = \frac{1}{S^{y}_{i}} \sum_{\ell=\frac{1-S^{y}_{i}}{2}}^{\frac{S^{y}_{i}-1}{2}} e^{-2\pi j d_s (m-n)\sin\left(\tilde{\alpha}_{i,k}+\frac{\ell\tilde{\theta}^{y}_{i,k}}{S^{y}_{i}-1}\right)}, \quad (17)$$

in which $\tilde{\alpha}_{i,k}$ represents the azimuth angle, while $\tilde{\theta}^{y}_{i,k}$ is the angular spread between the ith BS-cluster and the kth U-cluster in Y coordinate, and

$$[\tilde{\mathbf{R}}^{z}_{i,k}]_{(m,n)} = \frac{1}{S^{z}_{i}} \sum_{\ell=\frac{1-S^{z}_{i}}{2}}^{\frac{S^{z}_{i}-1}{2}} e^{-2\pi j d_s (m-n)\sin\left(\tilde{\phi}_{i,k}+\frac{\ell\tilde{\theta}^{z}_{i,k}}{S^{z}_{i}-1}\right)}, \quad (18)$$

where $\tilde{\phi}_{i,k}$ is the elevation angle between the ith BS-cluster and the U-cluster of user k and $\tilde{\theta}^{z}_{i,k}$ denotes the angular spread between them in the Z coordinate.

C. BIRTH-DEATH PROCESSES OF CLUSTERS AND SCATTERERS

Since both UEs and clusters are moving, the appearance and disappearance of clusters and scatterers on the array axis need to be included in the channel model. In order to insert this dynamic property of clusters and scatterers, a birth-death approach from a spatial evolution model is considered in this work. Let's consider only one cluster for each user and C clusters with S_i scatterers, $i = 1, 2, \ldots C$, for the ith BS-cluster, initially. Therefore, intending to implement the birth and death process, we propose to adopt two different strategies: *a*) PPP to model the birth and death of the scatterers for the kth U-cluster, and *b*) PCP on the BS side when new clusters with S_i scatterers are generated following the clustered Poisson process.

1) SCATTERERS BIRTH-DEATH AT THE UE SIDE

The scatterers can be modeled assumed to be PPP distributed in the XL-MIMO channel [15]. According to the birth and death Markovian process, the appearance and disappearance of scatterers are exponentially distributed. The *survival probability of the scatterers* between different U-clusters can be expressed as:

$$\Pr^{scat}_{srv} = e^{-\frac{\lambda_r d_s}{D}}, \quad (19)$$

where λ_r is the recombination rate of the scatterers, D is the coherence factor related to the environment, and d_s represents the spacing between the adjacent scatterers.

Then the *average number of newly generated scatterers* can be expressed as [14]:

$$\mu = \frac{\lambda_g}{\lambda_r}\left(1 - e^{-\frac{\lambda_r d_s}{D}}\right), \quad (20)$$

where λ_g represents the *rate of regeneration of scatterers*. A pseudo-code for birth and death process generation of scatterers is depicted in Algorithm 1.

Algorithm 1 Birth and Death Process of Scatterers

1: **Input** λ_r, λ_g, d_s, D, $\mathcal{S}_k$
2: **for** $\ell = 1 : S_k$ **do**
3: Determine if the scatterer survived
4: **if** $\mathcal{S}_k\{\ell\}$ survived **then**
5: $\mathcal{S}_k\{\ell\} = 1$
6: **else**
7: $\mathcal{S}_k\{\ell\} = 0$
8: **end if**
9: **end for**
10: New scatterers are generated according to Poisson process
11: Update the number of scatterers (S_k)
12: Update the set of scatterers for kth UE ($\mathcal{S}_k$)
13: **Output** $\mathcal{S}_k$

2) CLUSTERS BIRTH-DEATH AT THE BS SIDE

Similarly, the clusters at the BS side can be modeled assumed to be PCP distributed. The *survival probability of the clusters* can be expressed as:

$$\Pr^{clus}_{srv} = e^{-\frac{\lambda^{c}_{r} d_r}{D_c}}, \quad (21)$$

where λ^{c}_{r} is the recombination rate of the clusters, D_c is the coherence factor related to the environment on the array axis, and d_r represents the spacing between different antenna elements.

Therefore, the average number of newly generated clusters can be expressed as [14]:

$$\mu^{c} = \frac{\lambda^{c}_{g}}{\lambda^{c}_{r}}\left(1 - e^{-\frac{\lambda^{c}_{r} d_r}{D_c}}\right), \quad (22)$$

where λ^{c}_{g} represents the rate of regeneration of clusters.

The pseudo-code for birth and death generation of clusters is similar to that described in the Algorithm 1, simply substituting the entity ''scatterer'' by ''cluster'' and setting suitable parameter values, for the recombination and regeneration rates, coherence factor, and spacing between antennas.

We summarize the whole procedure for generating the proposed XL-MIMO channel model in Algorithm 2. Lines 4 and 6 generate the birth and death process of clusters and scatterers, respectively. After this, the VR size related to each cluster is determined in line 8. The correlation matrices are obtained as presented above according to the antenna adopted arrangement (ULA or UPA).

III. FIGURES OF MERIT: SINR, SE, CN AND FAVORABLE PROPAGATION

A. SPECTRAL EFFICIENCY (SE): LINEAR COMBINERS

Rewriting the expression in (1) as:

$$y = \sum_{k=1}^{K} h_k x_k + n, \quad (23)$$

and adopting linear receiver schemes at the BS, denoted by matrix $\mathbf{V} \in \mathbb{C}^{M\times K}$, the received signal is separated into K

Algorithm 2 Generation of XL-MIMO Channel With Birth and Death Process

Input M, K, d_r, d_s
Define $\mathbf{H} = \mathbf{0}_{M\times K}$
for $k = 1 : K$ **do**
  Update C (procedure similar to Algorithm 1)
  for $i = 1 : C$ **do**
    Update S_i (Algorithm 1)
    Define $\tilde{\mathbf{H}}_{i,k} = \mathbf{0}_{M\times S_i\times C}$
    Obtain $\mathcal{R}_i$
    Compute Υ_i in eq. (5) for ULA or (11) for UPA
    Compute $\boldsymbol{\rho}_i$ in eq. (6) for ULA or (12) for UPA
    Obtain azimuth and elevation angles
    Compute the correlation matrices
    Obtain $\mathbf{G}_i$
    Update $\tilde{\mathbf{H}}_{i,k}$ in (4)
  end for
  Compute visibility matrix $\mathbf{D}_k$ in (9)
  Obtain $\mathbf{g}_k$
  Update $\mathbf{H}(:, k)$ in (3)
end for
Output H

streams by multiplying y with the linear combining matrix:

$$\tilde{y} = \mathbf{V}^H y = \mathbf{V}^H \mathbf{H}\mathbf{x} + \mathbf{V}^H \mathbf{n}. \tag{24}$$

Therefore, from (24), the received signal for the kth user is given by:

$$\tilde{y} = v_k^H y = \underbrace{v_k^H h_k x_k}_{\text{desired signal}} + \underbrace{\sum_{j=1, j\neq k}^{K} v_k^H h_j x_j}_{\text{interuser interference}} + \underbrace{v_k^H n}_{\text{noise}}, \tag{25}$$

where v_k is the kth column of $\mathbf{V}$.

The *signal-to-interference-plus-noise ratio* (SINR) can be defined by:

$$\gamma_k = \frac{|\mathbf{v}_k^H \mathbf{h}_k|^2}{\sum_{j\neq k} |\mathbf{v}_k^H \mathbf{h}_j|^2 + \sigma_n^2 \|\mathbf{v}_k\|^2}. \tag{26}$$

Hence, the *overall SE* is defined according to:

$$SE = \left(1 - \frac{\tau}{T_c}\right) \cdot \sum_{k=1}^{K} \log_2(1 + \gamma_k) \quad \left[\frac{\text{bits}}{s \cdot \text{Hz}}\right], \tag{27}$$

where T_c is the channel coherence time, and τ is the period dedicated to training and channel estimation tasks.

In the sequel, we revisit some classical linear receivers deployed for the XL-MIMO channel analysis.

1) MAXIMUM-RATIO COMBINING (MRC)

This receiver simply neglects the effect of multiuser interference, aiming to maximize the received signal-to-noise ratio (SNR) of each user at the BS [22]. Following this policy, the MRC receiver is obtained by assigning $\mathbf{v}_k^{\text{MRC}} = \mathbf{h}_k$ in eq. (26), while the attained SINR for the kth user is:

$$\gamma_k^{\text{MRC}} = \frac{\|\mathbf{h}_k\|^4}{\sum_{j\neq k} |\mathbf{h}_k^H \mathbf{h}_j|^2 + \sigma_n^2 \|\mathbf{h}_k\|^2}. \tag{28}$$

Notice that the signal processing is very simple; however, as previously commented, this receiver has poor performance in the channel scenarios limited by the interference, since MRC does not consider the effect of multiuser interference.

2) ZERO-FORCING (ZF) COMBINER

Unlike MRC, zero-forcing receivers take into account account interuser interference but do not consider the effect of noise. The ZF combiner can eliminate multiuser interference by projecting each user vector onto the orthogonal complement of the interuser interference but assuming perfect channel state information (CSI) knowledge. The ZF combiner matrix is given by:

$$V^{\text{ZF}} = H(H^H H)^{-1}, \tag{29}$$

and the received SINR for the kth user deploying ZF combiner at BS is defined as:

$$\gamma_k^{\text{ZF}} = \frac{1}{\sigma_n^2 \left[(H^H H)^{-1}\right]_{kk}}, \tag{30}$$

where $[\cdot]_{kk}$ is the element of the kth row and kth column of the matrix.

3) MINIMUM MEAN-SQUARE ERROR (ZF) RECEIVER

The linear minimum mean-square error (MMSE) receiver aims to minimize the mean-square error between the estimate $v_k^H y$ and the transmitted signal x. Therefore, the MMSE combiner matrix is:

$$V^{\text{MMSE}} = (HH^H + \sigma_n^2 \mathbf{I}_M)^{-1} H. \tag{31}$$

Therefore, the received SINR of the kth user for the MMSE combiner results:

$$\gamma_k^{\text{MMSE}} = h_k^H \left(\sum_{i\neq k}^{K} h_i h_i^H + \sigma_n^2 \mathbf{I}_M\right)^{-1} h_k. \tag{32}$$

B. CONDITION NUMBER (CN)

The *condition number* (CN) of the channel matrix $\mathbf{H}$ is given by:

$$\kappa(\mathbf{H}) = \frac{\sigma_{\max}(\mathbf{H})}{\sigma_{\min}(\mathbf{H})} = \frac{|\lambda_{\max}(\mathbf{H})|}{|\lambda_{\min}(\mathbf{H})|}, \tag{33}$$

where $\sigma_{\max}(\mathbf{H})$ and $\sigma_{\min}(\mathbf{H})$ are maximal and minimal singular values of $\mathbf{H}$ respectively. If $\mathbf{H}$ is normal,[1] then the second equally holds, where $\lambda_{\max}(\mathbf{H})$ and $\lambda_{\min}(\mathbf{H})$ are maximal and minimal eigenvalues of $\mathbf{H}$ respectively.

In XL-MIMO, the CN is obtained considering the channel matrix formed by the VRs. The establishment of the cluster VRs channel link is obtained by evaluating the received signal

[1] A complex square matrix A is normal if it commutes with its conjugate transpose: $A^*A = AA^*$

at each antenna of the array, and only the subset of antennas that receive significant energy is selected to compose the cluster VR.

C. FAVORABLE PROPAGATION

Basically, favorable propagation is a massive MIMO channel characteristic that can be deployed to determine the level of interference the UEs cause to each other in the massive antenna configuration. Hence, one can define a metric to evaluate how near to the orthogonal are the channels. In addition, for the XL-MIMO system, we have the VR concept, in which only a part of the array receives the signal transmitted by the users. In fact, the multiuser interference for XL-MIMO tends to be less aggressive compared with massive MIMO case, since the VR overlap among users does not necessarily occur in all VR antennas.

In order to analyze the interference caused by UEs to each other when considering the double-scattering channel model, the inner product of the normalized channels h_k and h_j is given by:

$$\frac{h_k^H h_j}{\sqrt{\mathbb{E}\{||h_k||^2\}\mathbb{E}\{||h_j||^2\}}}, \tag{34}$$

that can be evaluated by simulation or experimentally. Hence, the variance of the normalized *favorable propagation* in (34) can be determined as [22]:

$$\mathbb{V}\text{ar}\left\{\frac{h_k^H h_j}{\sqrt{\mathbb{E}\{||h_k||^2\}\mathbb{E}\{||h_j||^2\}}}\right\} = \frac{\text{tr}(\mathbf{\Phi}_k\mathbf{\Phi}_j)}{\text{tr}(\mathbf{\Phi}_k)\text{tr}(\mathbf{\Phi}_j)}, \tag{35}$$

which expresses the variability of the kth and jth user channel realization regarding the perfect favorable propagation condition in eq. (34) (orthogonality), *i.e,* $h_k^H h_j = 0$ when $M \to \infty$.

Consequently, the interuser interference can be obtained by using the correlation matrix of each user. For the double-scattering (DS) correlated channel model, the correlation matrix for the kth user ($\mathbf{\Phi}_k$) can be calculated as [23]:

$$\mathbf{\Phi}_k = \text{tr}(\tilde{\mathbf{R}}_{i,k})\mathbf{R}_i. \tag{36}$$

This metric can determine how close are the spatial correlation matrices between the user k and j. Ideally, the variance in eq. (35) should be close to zero, which implies that the channels are practically orthogonal, thus the interuser interference is negligible.

IV. NUMERICAL RESULTS

In this section we evaluate and validate the proposed XL-MIMO channel models considering a) the effects of the number of visible clusters on the pos-combining SINR; b) favorable propagation effect and VR overlap; c) The attainable SE in XL-MIMO system equipped with ULA and UPA received antennas, and d) the effect of birth and death PPP and PCP over the XL-MIMO performance.

TABLE 1. Simulation parameters used to evaluate the impact of the number of visible clusters on the SINR.

Parameter	Value	Parameter	Value
M	256	K	[4; 16; 32; 64; 128; 256]
d_r	0.5λ	d_s	5λ
S_i	31	S_k	5
C	20	ψ_i	$\mathcal{LN}(\mu = 0.7, \sigma = 0.8)$ [dB/m]
θ_i	$7\pi/8$	$\tilde{\theta}_{i,k}$	$3\pi/4$
SNR	30 dB	$\alpha_i, \tilde{\alpha}_{i,k}$	$\mathcal{U}(-\pi/2, \pi/2)$
$\mathbb{E}[\mathbf{x}^2]$	1	n_b	[4; 8; 16]
f_c	2.6 GHz	Combiners	[MRC; ZF; MMSE]

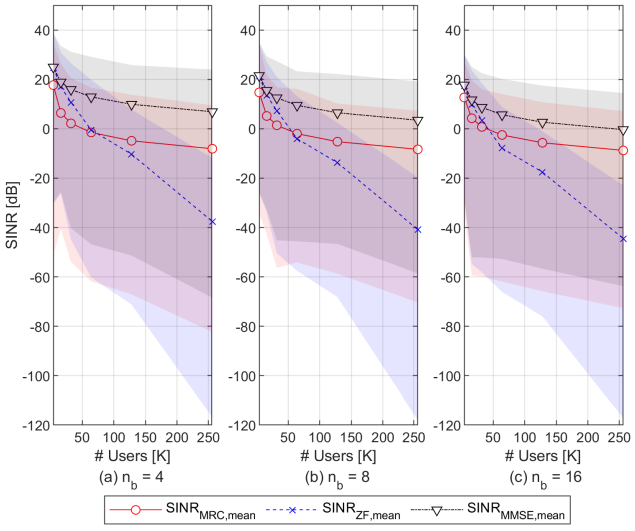

FIGURE 3. Minimum, maximum and average SINR for the XL-MIMO system with $M = 256$ ULA antennas and MRC, ZF and MMSE receivers. Number of visible clusters per user: a) $n_b = 4$; b) $n_b = 8$; c) $n_b = 16$.

A. IMPACT OF THE NUMBER OF VISIBLE CLUSTERS ON THE SINR

In this analysis, the average, minimum, and maximum SINR for the XL-MIMO channel is evaluated by increasing the number of users (K) under three linear receiver schemes (MRC, ZF, and MMSE) at the BS equipped with massive ULA antennas. Now, the number of visible BS-clusters (n_b) for the kth user is changed to measure how this parameter affects the SINR for different combiners. Table 1 shows the simulation parameters considered in this scenario. Moreover, the numerical results are obtained via Monte-Carlo simulation with 5000 realizations for each number of users.

Although the number of visible clusters varies, *i.e.*, $n_b \in \{4, 8, 16\}$, the total power received was held fixed. Therefore, this means that the user's VR is more spread out across the array, but with less power reaching each antenna element of the VR. As a result, as user's VR is higher, the trend is for multiuser interference to grow as well. Fig. 3 shows the numerical results obtained. As the MRC receiver does not take into account multiuser interference, seeking to maximize only the SNR of the received signal, in the three scenarios analyzed the SINR (minimum, maximum, and average) remains practically the same. As for the ZF and MMSE combiners, there is a slight decrease in the SINR as the number of visible clusters increases, which indicates that

TABLE 2. Simulation parameters for favorable propagation analysis and VR overlap in XL-MIMO with ULA arrangement.

Parameter	Value	Parameter	Value
M	256	K	2
d_r	0.5λ	d_s	5λ
S_i	31	S_k	5
C	2	ψ_i	$\mathcal{LN}(0.7; 0.8)$ [dB/m]
θ_i	$7\pi/8$	$\tilde{\theta}_{i,k}$	$3\pi/4$
α_1	$\pi/6$	α_2	$[-\pi : \pi/180 : \pi]$
$\tilde{\alpha}_{i,k}$	$\pi/6$	n_b	1
M_{VR}	50	VR overlap	[20%; 50%; 90%]

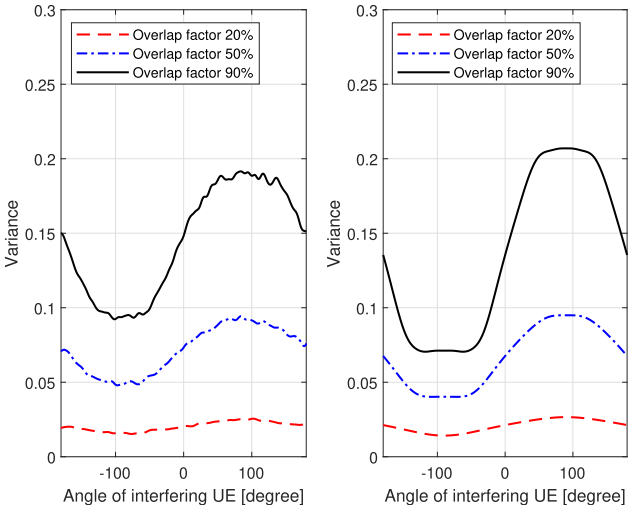

FIGURE 4. Interference evaluation for the XL-MIMO system with ULA arrangement and different VR overlap factors: (a) Monte-Carlo simulation obtained from left side of eq. (35) with $\mathcal{T} = 1000$ channel realizations; (b) Analytical expression provided by the right side of eq. (35).

the multiuser interference also increases, but this increase is not very significant and, then, the SE remains almost the same.

B. FAVORABLE PROPAGATION AND VR OVERLAP

In this section, the favorable propagation effect is obtained by evaluating eq. (35). For this analysis, three cases were considered in the numerical results: a) low VR overlap (20%); b) medium VR overlap (50%); c) high VR overlap (90%). For instance, considering $M_{\text{vr}} = 50$ antennas, the number of antennas in the VR for the users related to their respective clusters, 20% of VR overlap means that only 10 antenna elements are receiving power from both users.

To determine the impact of the XL-MIMO channel and the effect of the spatial correlation matrices between the user k and j, in the numerical simulations we have adopted the parameter values of Table 2. In the analyzed scenario of Fig. 4, the azimuth angle of one of the users is fixed in $\pi/6$ [rad], while for the other interfering user it is varied from $-\pi$ to π. Moreover, spreading angles are kept constant for both users, $\theta_i = 7\pi/8$ and $\tilde{\theta}_{i,k} = 3\pi/4$. In addition, the energy is exponentially attenuated from the center to the frontier of the VR, dictated by the factor ψ_i with a log-normal distribution as $\psi_i \sim \mathcal{LN}(\mu = 0.7, \sigma = 0.8)$ [dB/m].

TABLE 3. Simulation parameters adopted in the SE Analysis for XL-MIMO System with ULA and UPA Arrangement.

Parameter	Value	Parameter	Value
M	256	K	[4; 16; 32; 64; 128; 256]
d_r	0.5λ	d_s	5λ
C	20	ψ_i	$\mathcal{LN}(0.7, 0.8)$ [dB/m]
SNR	30 dB	$\alpha_i, \tilde{\alpha}_{i,k}$	$\mathcal{U}(-\pi/2, \pi/2)$
$\mathbb{E}[\mathbf{x}^2]$	1	τ/T_c	0.2
f_c	2.6 GHz	Combiners	[MRC; ZF; MMSE]
		ULA	
S_i	31	S_k	5
θ_i	$7\pi/8$	$\tilde{\theta}_{i,k}$	$3\pi/4$
		UPA	
S_i^y, S_i^z	31	S_k	5
θ_i^y, θ_i^z	$7\pi/8$	$\tilde{\theta}_{i,k}^y$, $\tilde{\theta}_{i,k}^z$	$3\pi/4$
α_i, $\tilde{\alpha}_{i,k}$	$\mathcal{U}(-\pi/2, \pi/2)$	ϕ_i, $\tilde{\phi}_{i,k}$	$\mathcal{U}(-\pi/2, \pi/2)$

From Fig. 4, the well-defined angles of interest related to the interfering UE can be identified. The interference (variance) generated by one user over the desired UE, given by eq. (35), is significantly larger when the interfering user is angularly located around the angle of the desired UE or closed to the mirror reflection angle $180° - 30° = 150°$. Furthermore, note that $\theta_i = 7\pi/8$ (157, 5°) and $\tilde{\theta}_{i,k} = 3\pi/4$ (135°) introduce a high angular standard deviation (ASD) σ_φ. So, the largest variance occurs when the UEs have different angles across the range between the angle of the desired UE and the mirror reflection angle. In addition, the VR overlap factor also significantly influences the variance, as expected, since this parameter directly impacts interuser interference.

C. SE OF XL-MIMO SYSTEM WITH ULA × UPA ARRANGEMENTS

In this subsection, for simplicity, a purely static approach to describe the XL-MIMO channel was adopted, *i.e.*, assuming a fixed number of scatterers and clusters. The aim is to evaluate the overall SE as a function of the number of users. Furthermore, we are considering a fixed SNR $= \frac{P}{\sigma_n^2}$, where P is the expected transmitting power of the users. Simulation parameters for the adopted scenario are shown in Table 3. Moreover, for the SE analysis, the numerical results were obtained via Monte-Carlo simulation averaged over $\mathcal{T} = 10^4$ realizations.

It is considered an XL-MIMO system with 256 antennas at the BS distributed in a ULA arrangement. Fig. 5 depicts results for the overall SE evaluated from eq. (27), by varying the number of users and deploying three different linear combiners: the MRC, ZF, and MMSE. The parameter $\frac{\tau}{T_c} = 0.2$ denotes that the channel estimation task requires 20% of the channel coherence time.

From Fig. 5 one can observe that the MRC receiver presents a poor performance in terms of SE. This behavior is expected, since MRC considers only the SNR, neglecting the multi-user interference, which grows significantly with the increase in the number of users. Moreover, note that the ZF combiner performs better than MRC up to $K = 32$ users ($M/K = 8$). However, from that point on, for the ZF is no longer able to separate the interference from the desired signal, and then ends up also suppressing the signal of interest

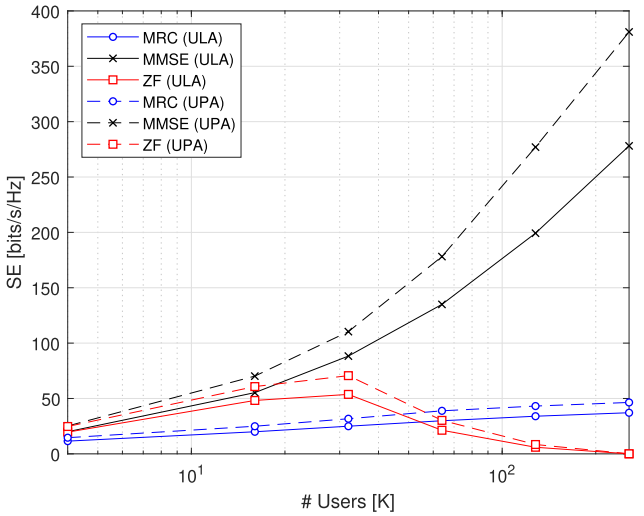

FIGURE 5. SE for XL-MIMO system with UPA *vs.* ULA antenna arrangements.

when trying to eliminate multiuser interference. As a result, the SE curve for the ZF combiner shows a trend reversal, decreasing until a value close to zero when the number of users reaches 128 or 256. Also, note that for $K = 64$ users, the MRC already exceeds the SE attained by the ZF, since the performance degradation of the ZF occurs quickly with the number of users increasing. Unlike MRC and ZF, the MMSE combiner performs greatly, even with the increase in the number of users, as expected. Observe that the MMSE receiver appears to have unlimited capacity w.r.t. the increase in the number of users, a feature previously observed in mMIMO systems [24].

The XL-MIMO system with UPA arrangement described in subsection II-B, which is a more effective array arrangement than ULA is also analyzed in this section. However, unlike the ULA model, we now also have the elevation angles $(\phi_i, \tilde{\phi}_{i,k})$ in addition to azimuth angles $(\alpha_i, \tilde{\alpha}_{i,k})$; the adopted range of values can be seen in Table 3. Beyond that, we have scatterers in both z and y coordinates in the ith BS-cluster. Thus, the channel model with UPA antenna arrangement has an extra degree of freedom compared to the ULA model.

Considering Fig. 5, the performance curves in terms of SE for the three combiners analyzed operating under the UPA arrangement presents a very similar behavior to that observed with the ULA. However, there are improvements in the SE performance of all combiners, with a gain of approximately 25 to 35%, compared with the ULA scenario; such SE improvement is more prominent with MMSE combiner under a higher user loading regime. Moreover, the MRC and ZF receivers performed worse compared to the MMSE in the scenario with a planar array arrangement; indeed, the ZF presents the same performance inversion problem seen previously. Again, the MMSE combiner presented the best performance among all, revealing an unlimited capacity trend with respect to the number of users.

Fig. 6 depicts the *condition number* (CN) for the channel matrix $\mathbf{H}$, as calculated by eq. (33), when the number of users increases and considering both linear and planar arrays. This is an interesting metric to explain the ZF receiver behavior since the condition number measures how well-conditioned is the analyzed matrix, which implies that the matrix is invertible or not. As the ZF needs to perform the calculation of the pseudoinverse of the channel matrix, it is essential that this matrix presents a low condition number value and, therefore its inverse can be computed with good accuracy. On the other hand, if the condition number is very large, the channel matrix is ill-conditioned. Additionally, three levels of channel correlation are considered for ULA and UPA arrangements: *i*) lowly correlated channel, *i.e.*, $\theta_i = 7\pi/8$, yielding $\mathbf{R}_i$ very close to the identity matrix; *ii*) moderate correlated channel with $\theta_i = \pi/3$, and *iii*) highly correlated channels under $\theta_i = \pi/8$. It is possible to notice that under moderate and high correlated channel scenarios, the *condition number* κ for both ULA and UPA arrangement is slightly higher than attainable under lowly correlated channels, but there is not a very significant difference, so it can be concluded that the effect of spatial correlation does not represent an impacting parameter in the condition number analysis of the XL-MIMO channel matrix $\mathbf{H}$. In this situation, the matrix is almost singular, and the computation of its inverse tends to present large numerical errors. Notice that in Fig. 6 for $K \geq 64$, the condition number κ reveals significant values increasing compared to the moderated or reduced system loading values, *i.e.*, $\mathcal{L} = \frac{K}{M} \geq \frac{64}{256} \approx 0.25$. Comparing the ULA array and the UPA, it is noticed that it presents similar κ values for $\mathcal{L} \leq \frac{32}{256} = 0.125$, however, from that on, the condition number for the ULA scenario grows much faster than UPA, tending to close values for a very high number of users or $\mathcal{L} \geq 1$. Thus, for $K > 32$ it is noticed that the channel matrix becomes poorly conditioned and, consequently, the performance with the ZF combiner is directly and heavily degraded.

D. BIRTH AND DEATH PPP AND PCP EFFECT OVER THE XL-MIMO CHANNEL

In this subsection, dynamic *vs.* quasi-static channel scenarios have been considered aiming at analyzing the effect of birth and death PPP and PCP modeling over the XL-MIMO performance. Table 4 summarizes the main parameter values considered in such analysis. Additionally, numerical results obtained via Monte-Carlo simulation were averaged over $\mathcal{T} = 10^4$ realizations for each number of users K, while ULA arrangement is adopted. Since the NLOS case is considered, the adopted parameter values are in accordance with the XL-MIMO channel measurements provided in [25] and [26].

In order to evaluate the effects and features of the parameters that define the PPP and PCP processes on the average SINR of the system, two scenarios have been considered for comparison purposes: *i*) *quasi-static* scenario, *i.e.*, the birth and death process for scatterers and clusters occurs much more slowly than the second case; and *ii*) *dynamic* scenario, in which the birth and death process happens more quickly, with a higher average number of newly generated and

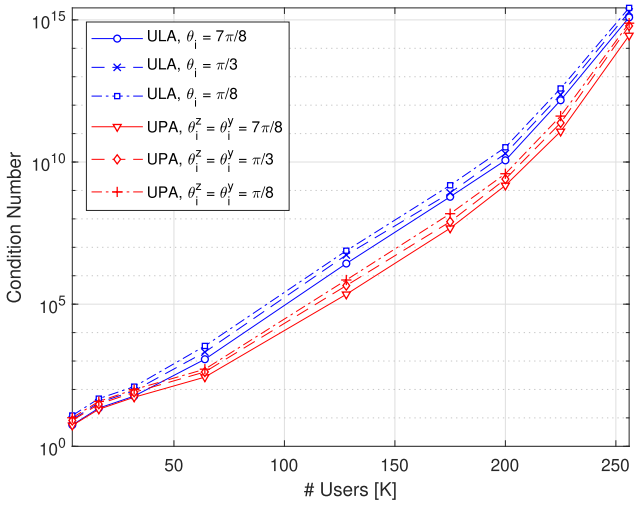

FIGURE 6. Averaged condition number of the H channel matrix with ULA and UPA arrangement over $\mathcal{T} = 1000$ channel realizations under low, moderate and high correlated channels.

TABLE 4. Simulation parameters used to evaluate the impact of birth and death PPP and PCP over the XL-MIMO SINR.

Parameter	Value	Parameter	Value
M	256	K	[4; 16; 32; 64; 128; 175; 200; 225; 256]
d_r	0.5λ	d_s	5λ
$S_{i,\text{ initial}}$	31	$S_{k,\text{ initial}}$	5
C_{initial}	20	ψ_i	$\mathcal{LN}(0.7,\ 0.8)$ [dB/m]
θ_i	$7\pi/8$	$\tilde{\theta}_{i,k}$	$3\pi/4$
SNR	30 dB	$\alpha_i, \tilde{\alpha}_{i,k}$	$\mathcal{U}(-\pi/2, \pi/2)$
f_c	2.6 GHz	Combiners	[MRC; ZF; MMSE]
Quasi-static scenario			
D	100 m	λ_R	2 m^{-1}
λ_G	20 m^{-1}	D_c	100 m
λ_R^c	8 m^{-1}	λ_G^c	80 m^{-1}
$\text{Pr}_{\text{srv}}^{\text{scat}}$	0.9885	$\text{Pr}_{\text{srv}}^{\text{clus}}$	0.9954
μ	0.1147	μ^c	0.0460
Dynamic scenario			
D	80 m	λ_R	4 m^{-1}
λ_G	20 m^{-1}	D_c	50 m
λ_R^c	16 m^{-1}	λ_G^c	200 m^{-1}
$\text{Pr}_{\text{srv}}^{\text{scat}}$	0.9716	$\text{Pr}_{\text{srv}}^{\text{clus}}$	0.9817
μ	0.1422	μ^c	0.2287

disappeared scatterers and clusters as well. For scenario *i*), the value of $D = D_c = 100$ m represents the scenario-dependent correlation factor for the scatterers and clusters, respectively. Moreover, $\lambda_R = 2\text{m}^{-1}$ and λ_R^c are set as 8m^{-1}, and the values of λ_G and λ_G^c are chosen as 20m^{-1} and 80m^{-1}, respectively. By using these values implies that the *survival probabilities* are 0.9885 for the scatterers and 0.9954 for the clusters. However, the *average number of newly generated scatterers is* $\mu = 0.1147$, while for the clusters such number is $\mu^c = 0.0460$, which results in a slow variation of the number of scatterers and clusters dictated by birth and death Poisson processes, denoted herein as a *quasi-static* setting. On the other hand, scenario *ii*) considers a more aggressive setup in terms of birth and death, since the *survival probabilities* are smaller, *i.e.*, $\text{Pr}_{srv}^{scat} = 0.9716$ and $\text{Pr}_{srv}^{clus} = 0.9817$, but the average number of newly generated scatterers and clusters are also increased. The aim of analyzing such channel modeling

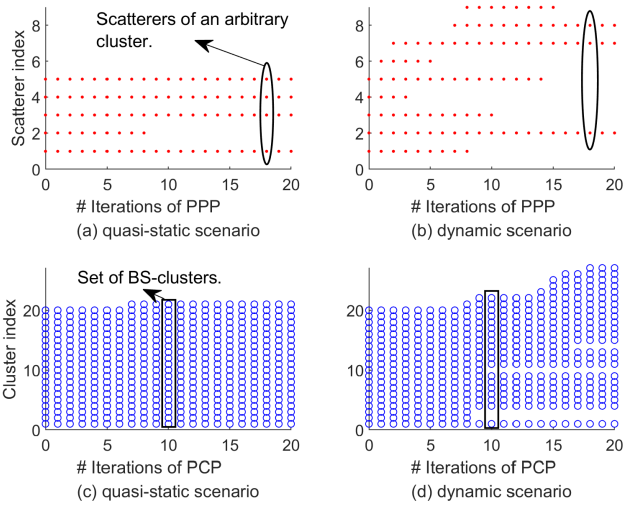

FIGURE 7. Birth and death PPP and PCP over the XL-MIMO ULA arrangement. $\mathcal{T} = 20$ realizations.

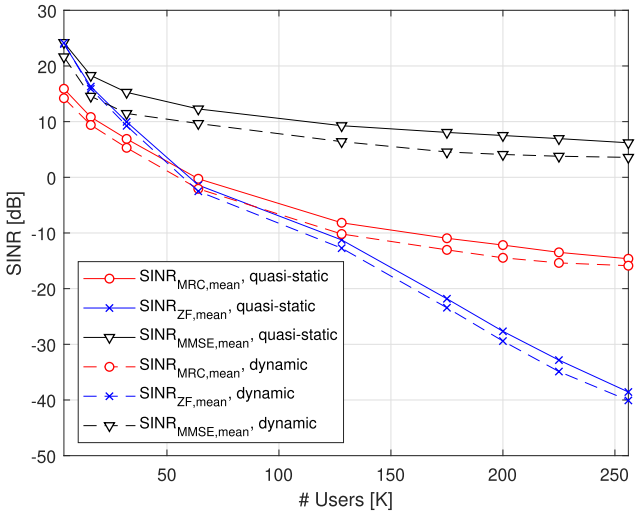

FIGURE 8. Average SINR with birth and death PPP and PCP over the XL-MIMO ULA arrangement. $\mathcal{T} = 10^4$ channel realizations.

is to characterize a real dynamic scenario with different levels of mobility of both the user and the surrounding objects.

Fig. 7 illustrates the birth and death Poisson process with 20 realizations in both analyzed scenarios. The dots on Fig. 7 represent the active scatterers, while circles are the clusters. Note that their disappearance demonstrates that they have been inactivated/death. From that, it is possible to observe that the birth and death rate for the quasi-static scenario is much lower compared to the dynamic scenario adopted in this work.

Comparing the average SINR depicted in Fig. 3 with the *quasi-static* channel scenario shown in Fig. 8, one can notice that the three receiver schemes present a very similar performance obtained in the static scenario. However, under the *dynamic* birth and death process setup, there is an intrinsic degradation of the SINR. While the MRC and ZF receivers show a decrease of 1 to 2 dB in SINR, the MMSE was even more affected, presenting a degradation of 3 to 4 dB in SINR. Notice the same performance inversion observed in the SE

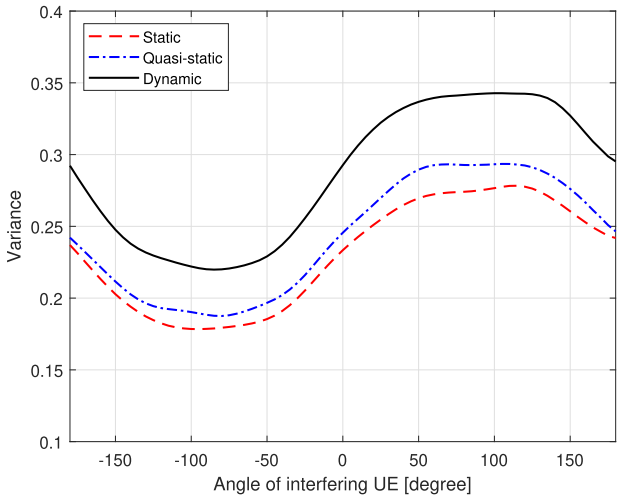

FIGURE 9. Interference for the XL-MIMO system with ULA arrangement at the static (without birth and death process), quasi-static and dynamic scenarios.

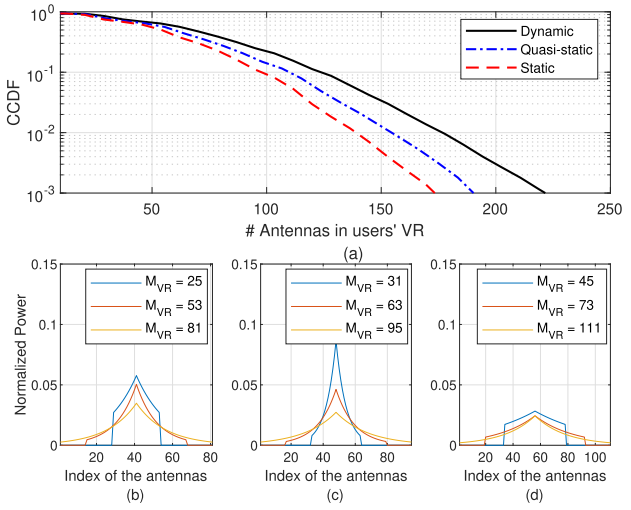

FIGURE 10. User's VR size for the XL-MIMO system with ULA arrangement. a) CCDF of the number of antennas in users' VR; power profile of user's VR in three different scenarios: b) static; c) quasi-static; d) dynamic.

of Fig. 5 regarding ZF and MRC when $K \geq 64$ also occurs in Fig. 8 in terms of average SINR of the XL-MIMO system equipped with the ZF and MRC combiners.

The impact of the birth and death process on the channel correlations is evaluated in Fig. 9 by mean of eq. (35). For this, a Monte-Carlo simulation is carried out varying the angle of interfering UE in three different scenarios: *static*, with a fixed number of scatterers and clusters (without the birth and death process); *quasi-static* and *dynamic*, in which we adopt the same parameters depicted in Table 4. From Fig. 9, observe that the static and quasi-static scenarios reveal a very similar behavior, although it is noted that there is a small increase in the level of interference. In the dynamic scenario, however, there is a more significant increase ($\approx$ 30%) in the interference level when compared to the static channel scenario, due to the higher birth and death rate of scatterers and clusters, indicating that this phenomenon directly affects the level of interference in the XL-MIMO multiuser channels.

Next, we analyze the *effect of birth and death process on the VR size* and *its power distribution*. For this, we consider the same parameters presented in Table 4, excepting that $K = 128$ and $\mathcal{T} = 10^5$ channel realizations. The number of antennas in users' VR (M_{vr}) are evaluated in the same scenarios adopted above (static, quasi-static and dynamic). Note that while the rate of the birth and death is increased, M_{vr} also shows an increasing trend. This also directly impacts the power distribution within the VR antennas, as seen in the figures 10(b), 10(c) and 10(d), representing static, quasi-static and dynamic scenarios, respectively. We also have selected three M_{vr} values (low, medium an high) for each scenario according to the CCDF curves (CCDF $\approx$ [0.2; 0.5; 0.9]). As the normalized power is considered, it can be observed that when the VR size increased the the energy peak in the center of the VR is smaller and the energy received in the rest of the VR also tends to be smaller.

V. CONCLUSION

In this paper we propose a double-scattering channel model for XL-MIMO systems equipped with UPA and ULA antennas arrangements, aiming to provide analysis tools for evaluating features and performance of such a massive MIMO system configurations, also taking into account linear receiver schemes for realistic system application scenarios.

The XL-MIMO with UPA arrangement reveals a SE performance gain of $\approx$ 35% in comparison to the ULA counterpart. This can be explained by the fact that the XL-MIMO equipped with UPA presents an extra spatial degree of freedom in relation to the ULA, which leads to a lower level of correlation between users, reducing interuser interference accordingly. Moreover, numerical results unveil the performance of with the ZF combiner is greatly affected in medium-highly loaded and crowded massive MIMO scenarios, *i.e.*, $\mathcal{L} = \frac{K}{M} \geq \frac{64}{256} \approx 0.25$, leading to a remarkable performance degradation in such context. Even though the MRC does not present the same problems as the ZF receiver, the MRC combiner also ends up with a very limited SE performance, which is expected in crowded scenarios since the inter-user interference is not taken into account in such receiver. Unlike ZF and MRC combiners, the MMSE combiner presents an optimal performance in both analyzed types of massive arrays, resulting in unlimited capacity regarding the number of users, even under crowded configurations, *i.e.* $\mathcal{L} \approx 1$.

The proposed birth and death Poisson processes modeling the rising and the disappearance appearance and vanishing of scatterers and clusters in the XL-MIMO channels with ULA and UPA arrangements were analyzed to emulate a dynamic system scenario, where both user and the surrounding objects present a certain level of mobility. Hence, the analyzed linear receivers reveal an SINR performance degradation with the increase of the birth and death rate of scatterers and clusters, a clear indication that the mobility directly affects the level of interference in the doubly scattered XL-MIMO multiuser channels. This effect is 3 to 4 dB for the MMSE, while the ZF

and MRC receivers present a decrease of around 1 to 2 dB in SINR for the considered dynamic configuration.

In this paper, we focus on the analysis of near-field propagation condition, *i.e.*, the spatial non-stationarities, including the VR effects, and also considering the *birth* and *death processes* to accordingly model double-scattering XL-MIMO channels with uniform distributions of antennas and scatterers, for simplicity. Future works include investigating irregular distributions of scatterers to represent more realistic scenarios, as well as proposed appropriate models that consider hardware constraints, such as radio frequency impairment and hardware response, and all-digital or hybrid structures.

REFERENCES

[1] E. Björnson, L. Sanguinetti, H. Wymeersch, J. Hoydis, and T. L. Marzetta, "Massive MIMO is a reality—What is next? Five promising research directions for antenna arrays," *Digit. Signal Process.*, vol. 94, pp. 3–20, Nov. 2019.

[2] C. D. Alwis, A. Kalla, Q.-V. Pham, P. Kumar, K. Dev, W.-J. Hwang, and M. Liyanage, "Survey on 6G frontiers: Trends, applications, requirements, technologies and future research," *IEEE Open J. Commun. Soc.*, vol. 2, pp. 836–886, 2021.

[3] H. Lu and Y. Zeng, "Near-field modeling and performance analysis for multi-user extremely large-scale MIMO communication," *IEEE Commun. Lett.*, vol. 26, no. 2, pp. 277–281, Feb. 2022.

[4] S. Gunnarsson, J. Flordelis, L. Van Der Perre, and F. Tufvesson, "Channel hardening in massive MIMO: Model parameters and experimental assessment," *IEEE Open J. Commun. Soc.*, vol. 1, pp. 501–512, 2020.

[5] H. Lu and Y. Zeng, "How does performance scale with antenna number for extremely large-scale MIMO?" in *Proc. IEEE Int. Conf. Commun. (ICC)*, Jun. 2021, pp. 1–6.

[6] A. Ali, E. de Carvalho, and R. W. Heath, Jr., "Linear receivers in non-stationary massive MIMO channels with visibility regions," *IEEE Wireless Commun. Lett.*, vol. 8, no. 3, pp. 885–888, Jun. 2019.

[7] S. Chen, S. Sun, G. Xu, X. Su, and Y. Cai, "Beam-space multiplexing: Practice, theory, and trends, from 4G TD-LTE, 5G, to 6G and beyond," *IEEE Wireless Commun.*, vol. 27, no. 2, pp. 162–172, Apr. 2020.

[8] Y. Han, S. Jin, C.-K. Wen, and X. Ma, "Channel estimation for extremely large-scale massive MIMO systems," *IEEE Wireless Commun. Lett.*, vol. 9, no. 5, pp. 633–637, May 2020.

[9] X. Yang, F. Cao, M. Matthaiou, and S. Jin, "On the uplink transmission of extra-large scale massive MIMO systems," *IEEE Trans. Veh. Technol.*, vol. 69, no. 12, pp. 15229–15243, Dec. 2020.

[10] V. C. Rodrigues, A. Amiri, T. Abrão, E. de Carvalho, and P. Popovski, "Low-complexity distributed XL-MIMO for multiuser detection," in *Proc. IEEE Int. Conf. Commun. Workshops (ICC Workshops)*, Jun. 2020, pp. 1–6.

[11] L. M. Taniguchi and T. Abrão, "Stochastic channel models for massive and extreme large multiple-input multiple-output systems," *Trans. Emerg. Telecommun. Technol.*, vol. 31, no. 9, Sep. 2020, Art. no. e4099. [Online]. Available: https://onlinelibrary.wiley.com/doi/abs/10.1002/ett.4099

[12] H. Jiang, Z. Zhang, L. Wu, J. Dang, and G. Gui, "A 3-D non-stationary wideband geometry-based channel model for MIMO vehicle-to-vehicle communications in tunnel environments," *IEEE Trans. Veh. Technol.*, vol. 68, no. 7, pp. 6257–6271, Jul. 2019.

[13] A. Amiri, S. Rezaie, C. N. Manchón, and E. De Carvalho, "Distributed receiver processing for extra-large MIMO arrays: A message passing approach," *IEEE Trans. Wireless Commun.*, early access, Sep. 28, 2021, doi: 10.1109/TWC.2021.3114380.

[14] J.-Q. Chen, Z. Zhang, T. Tang, and Y.-Z. Huang, "A non-stationary channel model for 5G massive MIMO systems," *Frontiers Inf. Technol. Electron. Eng.*, vol. 18, no. 12, pp. 2101–2110, Dec. 2017.

[15] S. Wu, C.-X. Wang, E.-H. M. Aggoune, M. M. Alwakeel, and X. You, "A general 3-D non-stationary 5G wireless channel model," *IEEE Trans. Commun.*, vol. 66, no. 7, pp. 3065–3078, Jul. 2018.

[16] C. F. Lopez and C.-X. Wang, "A study of 2D non-stationary massive MIMO channels by transformation of delay and angular power spectral densities," *IEEE Trans. Veh. Technol.*, vol. 69, no. 12, pp. 14212–14224, Dec. 2020.

[17] C. F. López, C.-X. Wang, and Y. Zheng, "A 3D non-stationary wideband massive MIMO channel model based on ray-level evolution," *IEEE Trans. Commun.*, vol. 70, no. 1, pp. 621–634, Jan. 2022.

[18] Z. Ma, B. Ai, R. He, Z. Zhong, and M. Yang, "A non-stationary geometry-based MIMO channel model for millimeter-wave UAV networks," *IEEE J. Sel. Areas Commun.*, vol. 39, no. 10, pp. 2960–2974, Oct. 2021.

[19] E. D. Carvalho, A. Ali, A. Amiri, M. Angjelichinoski, and R. W. Heath, Jr., "Non-stationarities in extra-large-scale massive MIMO," *IEEE Wireless Commun.*, vol. 27, no. 4, pp. 74–80, Aug. 2020.

[20] X. Gao, F. Tufvesson, and O. Edfors, "Massive MIMO channels—Measurements and models," in *Proc. Asilomar Conf. Signals, Syst. Comput.*, Nov. 2013, pp. 280–284.

[21] D. W. M. Guerra, R. M. Fukuda, R. T. Kobayashi, and T. Abrão, "Efficient detectors for MIMO-OFDM systems under spatial correlation antenna arrays," *ETRI J.*, vol. 40, no. 5, pp. 570–581, Oct. 2018. [Online]. Available: https://onlinelibrary.wiley.com/doi/abs/10.4218/etrij.2018-0005

[22] E. Björnson, J. Hoydis, and L. Sanguinetti, *Massive MIMO Networks: Spectral, Energy, and Hardware Efficiency*. Boston, MA, USA: Now, 2017.

[23] Q.-U.-A. Nadeem, A. Kammoun, M. Debbah, and M.-S. Alouini, "Asymptotic analysis of RZF over double scattering channels with MMSE estimation," *IEEE Trans. Wireless Commun.*, vol. 18, no. 5, pp. 2509–2526, May 2019.

[24] E. Björnson, J. Hoydis, and L. Sanguinetti, "Massive MIMO has unlimited capacity," *IEEE Trans. Wireless Commun.*, vol. 17, no. 1, pp. 574–590, Jan. 2018.

[25] S. Payami and F. Tufvesson, "Channel measurements and analysis for very large array systems at 2.6 GHz," in *Proc. 6th Eur. Conf. Antennas Propag. (EUCAP)*, Mar. 2012, pp. 433–437.

[26] X. Gao, F. Tufvesson, O. Edfors, and F. Rusek, "Measured propagation characteristics for very-large MIMO at 2.6 GHz," in *Proc. Conf. Rec. 46th Asilomar Conf. Signals, Syst. Comput. (ASILOMAR)*, Nov. 2012, pp. 295–299.

DAVID WILLIAM MARQUES GUERRA received the B.S. and M.Sc. degrees in electrical engineering from the State University of Londrina, Brazil, in 2017 and 2019, respectively, where he is currently pursuing the Ph.D. degree in electrical engineering. His research interests include telecommunication systems, more precisely in wireless communications and signal processing, including multicarrier systems, massive MIMO, XL-MIMO, 5G, 6G, machine learning, and the optimization aspects of communications systems and signals.

TAUFIK ABRÃO (Senior Member, IEEE) received the B.S., M.Sc., and Ph.D. degrees in electrical engineering from the Polytechnic School, University of São Paulo, São Paulo, Brazil, in 1992, 1996, and 2001, respectively. Since March 1997, he has been with the Communications Group, Department of Electrical Engineering, Londrina State University, Paraná, Brazil, where he is currently an Associate Professor of telecommunications and the Head of the Telecommunication and Signal Processing Laboratory. From July 2018 to October 2018, he was with the Connectivity Section, Aalborg University, as a Guest Researcher. In 2012, he was an Academic Visitor with the Southampton Wireless Research Group, University of Southampton, U.K. His research interests include massive and XL-MIMO, RIS-aided communications, URLLC, mMTC, random access protocols, detection and estimation, NOMA systems, cooperative communication, resource allocation, machine learning-aided communications, and optimization techniques for 5G and 6G wireless systems. He has also served as an Associate Editor for the IEEE Systems Journal, the IEEE Transactions on Vehicular Technology, the *IET Electronics Letters*, the *et al.* (Wiley) journal, and the *AEUe* (Elsevier). Previously, he served as an AE for the IEEE Communication Surveys and Tutorials (2013–2017), IEEE Access (2016–2019), and the *IET Signal Processing* (2018–2020).